Parameterizing air-sea gas transfer velocity with dissipation

L. Esters[1], S. Landwehr[1] , G. Sutherland[2] , T. G. Bell[3] , K. H. Christensen[4] , E. S. Saltzman[5], S. D. Miller[6] , and B. Ward[1]

[1]AirSea Laboratory, School of Physics and Ryan Institute, National University of Ireland, Galway, Galway, Ireland, [2]Department of Mathematics, University of Oslo, Oslo, Norway, [3]Plymouth Marine Laboratory, Plymouth, United Kingdom, [4]Norwegian Meteorological Institute, Oslo, Norway, [5]Earth System Science, University of California, Irvine, California, USA, [6]Atmospheric Sciences Research Center, State University of New York at Albany, Albany, New York, USA

Abstract The air-sea gas transfer velocity k is frequently estimated as an empirical function of wind speed. However, it is widely recognized that k depends on processes other than wind speed alone. The small-eddy model, which describes periodic events of small eddies disturbing the sea surface with water from below, suggests a direct relation between k and the dissipation rate of turbulent kinetic energy ϵ at the air-sea interface. This relation has been proven both in laboratories and in the field in various freshwater and coastal environments, but to date has not been verified in open ocean conditions. Here, concurrent North Atlantic field observations of ϵ and eddy covariance measurements of DMS and CO_2 air-sea gas flux are presented. Using ϵ measurements, we compare the small-eddy model at various depths to previously published observations. Extrapolating the measured ϵ profiles to the thickness of the viscous sublayer allows us to formulate a function of k that depends solely on the water side friction velocity u_{*_w}, which can be inferred from direct eddy covariance measurements of the air-side friction velocity u_{*_a}. These field observations are generally consistent with the theoretical small-eddy model. Utilizing a variable Schmidt number exponent in the model, rather than a constant value of $\frac{1}{2}$ yields improved agreement between model and observations.

1. Introduction

The oceans and the atmosphere form a tightly coupled system and the processes at the interface play an important role in air-sea gas exchange. Estimating the fluxes between the atmosphere and the ocean requires an understanding of the physical processes on both sides of the interface.

The magnitude and direction of the gas flux F at the interface are typically determined by the air-sea difference in the partial pressure of a particular gas ΔP and by the transfer velocity K, which describes the efficiency in the transport process using the following equation:

$$F = K \, s \, \Delta P, \tag{1}$$

where K is the total gas transfer velocity and s is the solubility of a gas, which can be determined from sea surface temperature and salinity [*Weiss*, 1974; *Wanninkhof et al.*, 2009]. High precision field measurements of ΔP are readily available [e.g., *Bakker et al.*, 2016; *Watson et al.*, 2009; *Lana et al.*, 2011], but direct measurements of F are more challenging, and K is frequently parameterized as a function of wind speed.

K combines the effects of processes at the air as well as the water side of the air-sea interface. The inverses of the transfer velocities are the gas transfer resistances. The air side and water side resistances can be added to obtain the total resistance:

$$\frac{1}{K} = \frac{1}{k_a} + \frac{1}{k_w}, \tag{2}$$

where k_a and k_w denote the air side and the water side gas transfer velocity expressed in the same units (typically of the water side gas transfer velocity). For CO_2 and DMS under the conditions of the Knorr11 study, $k_a \gg k_w$ and $K \approx k_w$ can be approximated to within 6% [*Bell et al.*, 2013]. In the following, we refer to the water side gas transfer velocity as k.

The most commonly used parameterizations of k are based on functions of wind speed normalized to 10 m height: $k = f(u_{10N})$ [*Liss and Merlivat*, 1986; *Wanninkhof*, 1992; *Wanninkhof and McGillis*, 1999; *Nightingale et al.*, 2000; *Sweeney et al.*, 2007; *Goddijn-Murphy et al.*, 2012]. Wind speed is a readily available parameter from both in situ and satellite observations and directly or indirectly influences most of the physical processes controlling the air-sea gas exchange. However, the most commonly used parameterizations are empirical fits to observations of k and do not rely on the underlying physics of the exchange process. *Wanninkhof* [1992] used the global bomb ^{14}C data and combined it with global averaged wind speeds to which he scaled a quadratic relationship $k = f(u_{10})$. This and further global quadratic relations feature a zero intercept [*Nightingale et al.*, 2000; *Sweeney et al.*, 2007], which leads to the assumption of zero gas exchange at low wind speeds. It is known, however, that buoyancy effects, chemical enhancement, surface waves, and micro breaking events force gas exchange to occur even at low wind speeds [e.g., *Sutherland and Melville*, 2015; *Wang and Liao*, 2016]. *McGillis et al.* [2001, 2004] accounted for these effects by adding a constant value of k to wind speed-based parameterizations. Additionally, bubble entrainment and breaking waves at high wind speeds lead *McGillis et al.* [2001] to propose a cubic instead of quadratic wind speed dependence of k.

The empirical wind speed-based relations allow for approximate estimates of k, but they do not incorporate the complexity of the physics at the air-sea interface. Therefore, a physically based parameterization is desirable. The National Oceanic and Atmospheric Administration/Coupled-Ocean Atmospheric Response Experiment (NOAA/COARE) air-sea gas transfer algorithm [*Fairall et al.*, 2000], which is based on the COARE Bulk Flux Algorithm [*Fairall et al.*, 1996] with additional implication of the surface renewal theory [*Soloviev and Schlüssel*, 1994] incorporates physical mechanisms of gas transfer to calculate k from readily available input variables.

Parameterizing k directly with the dissipation rate of turbulent kinetic energy ϵ offers a further opportunity to fulfil the requirement of a physically based parameterization, as turbulence is the major physical mechanism that controls k [e.g., *Wanninkhof et al.*, 2009]. *Lamont and Scott* [1970] derived a direct relation between k and surface ϵ_0 using the surface renewal theory [*Higbie*, 1935; *Danckwerts*, 1951]. This theory describes periodic events of small eddies disturbing the sea surface with water from below (small-eddy model—SEM). Following *Lamont and Scott* [1970], k can be parameterized by:

$$k = A \mathrm{Sc}^{-n} (\epsilon_0 \, v)^{1/4}, \tag{3}$$

where A is a proportionality constant, $\mathrm{Sc} = v/D$ is the Schmidt number, which is defined as the ratio of the kinematic viscosity of water v to molecular diffusivity of the trace gas in water D, and n is the Schmidt number exponent. *Lamont and Scott* [1970] formulated equation (3) with a Schmidt number exponent of $n = \frac{1}{2}$ by predicting the time scales in the surface renewal gas/liquid transport model. For flat surfaces which behave hydrodynamically analogous to solid/liquid interfaces a Schmidt number exponent of $n = \frac{2}{3}$ is assumed [*Davies*, 1972]. Flat surfaces can exist for open ocean conditions under either very low wind conditions or in the presence of surface films at low to medium wind speeds. In reality, the sea surface might be partially covered with surfactants and waves might occur in different stages, and thus n can be assumed to vary between $\frac{1}{2}$ for a wavy, surfactant-free surface and $\frac{2}{3}$ for a flat surface depending on the conditions [*Deacon*, 1977; *Jähne et al.*, 1987].

Studies in the field [*Zappa et al.*, 2007; *Tokoro et al.*, 2008; *Vachon et al.*, 2010; *Wang et al.*, 2015; *Gålfalk et al.*, 2013] and in laboratories [*Asher and Pankow*, 1986; *Moog and Jirka*, 1999] have shown the SEM to hold well in various conditions. Measurements of k and ϵ have been carried out in rivers, lakes, estuaries, coastal oceans, and the model-world Biosphere 2, under a wide range of forcings from wind, tides, and rain [*Gålfalk et al.*, 2013; *Zappa et al.*, 2007; *Tokoro et al.*, 2008; *Vachon et al.*, 2010; *Wang et al.*, 2015]. The instrumental setup varied for the different studies, and ϵ was measured at various depths below the surface. No investigations have been carried out in the open ocean relating k to ϵ.

Direct eddy covariance measurements of DMS and CO_2 air-sea fluxes aboard the RV Knorr and simultaneous measurements of ϵ from the upwardly rising Air-Sea Interaction Profiler (ASIP) in the North Atlantic provide the opportunity to apply equation (3) for the first time in the open ocean. In section 2, the ASIP data and the flux measurements are described. These measurements are used to validate the SEM, and the results are presented in section 3. We compare the surface values of ϵ from four ASIP deployments (283 samples in total) to the values of k derived from direct DMS and CO_2 flux and air-sea concentration difference measurements. The applicability of the SEM is compared to commonly used wind speed-based parameterizations in

section 3.2 and further investigations on the proportionality constant are presented in section 3.3. Section 4 summarizes the results and presents conclusions.

2. Methods

Measurements were taken during the Knorr11 field campaign in the North Atlantic, aboard the RV Knorr from late June to mid-July 2011, leaving and returning to Woods Hole, USA [see *Scanlon and Ward*, 2013; *Bell et al.*, 2013; *Sutherland et al.*, 2013; *Christensen et al.*, 2013; *Sutherland et al.*, 2014a; *O'Sullivan et al.*, 2015; *Scanlon and Ward*, 2016; *Scanlon et al.*, 2016, for further details].

To expand the analysis, the observations from the North Atlantic are compared to measurements of k in the Pacific Ocean during the Surface Ocean Aerosol Production (SOAP) cruise [*Landwehr et al.*, 2013; *Bell et al.*, 2015]. The cruise was carried out in February–March 2012 east of New Zealand aboard the RV Tangaroa. Similarly to the Knorr11 cruise, sampling was performed in highly productive algal blooms.

2.1. Air-Sea Fluxes

The eddy covariance system consisted of two sonic anemometers (Campbell CSAT3), measuring the three-dimensional wind speed, and two inertial motion sensors (Systron Donner Motion Pack II) that recorded the platform motion. In order to minimize the effect on air-flow distortion the covariance system was mounted on the bow mast of the ship at a height of about 13.6 m above the mean water level. *O'Sullivan et al.* [2015] provides a detailed study of the effects of air-flow distortion on the measurements on the RV Knorr. For this study, the data set was restricted to measurements where the apparent relative wind direction was less than $90°$ from the bow for both CO_2 and DMS.

Air sampling inlets were mounted between the two anemometers at the same height and provided two closed chamber gas analyzer systems, which are described in detail in *Miller et al.* [2010] and *Bell et al.* [2013], for CO_2 and DMS, respectively. These publications also provide descriptions of the measurements of the air-sea concentration gradients of CO_2 and DMS. The CO_2 and DMS concentration in seawater were continuously measured using equilibrator systems [*Miller et al.*, 2010; *Bell et al.*, 2013; *Saltzman et al.*, 2009]. In these systems, air was equilibrated with uncontaminated surface sea water from the ship's bow pumping system, and passed through a gas analyzer.

The apparent wind speed was corrected for platform motion and mean tilt of the air-flow as described in *Landwehr et al.* [2015], and was then used to calculate the air-side friction velocity $u_{*a} = \sqrt{(\overline{w'u'})^2 + (\overline{w'v'})^2}$, where u, v, and w are the along wind and the horizontal and vertical cross wind components of the wind vector with u', v', w' representing the derivation of the mean in the respective wind components: $u = \overline{u} + u'$, with $\overline{u}$ referring to the mean velocity.

The gas fluxes F_{DMS} and F_{CO_2} were calculated as covariances of the vertical wind speed component w and the gas mixing ratios: $F_x = \rho_a \overline{w'x'}$, where ρ_a is the dry air density.

The 10 min averaged gas flux and concentration gradient measurements were used to obtain the total gas transfer velocity K via equation (1), which in the case of CO_2 and DMS well approximates the water side transfer velocity k. In order to account for the influence of the sea surface temperature and salinity the transfer velocities were normalized to a Schmidt number of 660, which corresponds to CO_2 at 25°C:

$$k_{660} = k \cdot \left(\frac{660}{Sc_x}\right)^{-n}, \tag{4}$$

where Sc_x refers to the Schmidt number at the in situ seawater temperature and salinity for either DMS or CO_2. In the following, the normalized gas transfer velocities k_{660} are referred to as k_{DMS} and k_{CO_2} for DMS and CO_2, respectively.

2.2. Measurements and Scaling of Surface Turbulence

The Air-Sea Interaction Profiler (ASIP) is an autonomous, upwardly rising, microstructure profiler [*Ward et al.*, 2014]. It was specially developed to study the upper few meters of the ocean and provides data from a maximum depth of 100 m to the ocean surface. The profiler being autonomous allows for measurements in an

undisturbed environment. ASIP is equipped with two shear probes, which allow estimations of ϵ with a vertical resolution of approximately 0.5 m [*Sutherland et al.*, 2013].

Ideally, ϵ should be measured immediately below the air-sea interface to represent the physical conditions of the water surface. However, the shear probe measurements were used to calculate ϵ over 1 second intervals, which for a rise velocity of 0.5 m s^{-1}, resulted into a 0.5 m resolution [*Ward et al.*, 2014]. The profiles were extrapolated to the air-sea interface. *Lorke and Peeters* [2006] scaled ϵ with the turbulent kinetic energy TKE production by the wind-stress, using the law of the wall (LOW), which assumes the oceanic boundary layer to behave as a shear-driven layer beneath a rigid and flat surface. The total stress in this layer is supposed to be constant leading to an increasing log-linear velocity profile with an inversely decreasing ϵ:

$$\epsilon_{LOW}(z) = \frac{u_{*_w}^3}{\kappa z},\qquad(5)$$

where $\kappa \approx 0.41$ is the von Kármán constant, z is the measurement depth, and u_{*_w} is the water side friction velocity derived from direct eddy covariance measurements of the air-side friction velocity u_{*_a} via the law of momentum conservation ($u_{*_a}^2 \rho_a = u_{*_w}^2 \rho_w$ with ρ_w being the water density). In the following, the water side friction velocity is referred to as u_*. The LOW is a basic similarity scaling, which does not take waves into account and thus might not be adequate of describing ϵ in presence of breaking waves.

The LOW reproduces the shape of the measured ϵ profiles during the Knorr11 cruise relatively well but overestimates the observed values of ϵ within the mixing layer (XLD) for the majority of ASIP profiles (Figure 1). The XLD is the ocean surface layer of active mixing and its depth is defined as the depth at which ϵ falls to a background level of $\epsilon = 10^{-9}$ m^2 s^{-1} [*Brainerd and Gregg*, 1995; *Sutherland et al.*, 2014b]. Through a detailed analysis of ϵ measured during the Knorr11 cruise, *Sutherland et al.* [2013] found that the LOW predicts ϵ within an order of magnitude, but with a tendency to overestimate the observed ϵ. Previous observations found that the LOW underestimated observed dissipation by 1–2 orders of magnitude [*Kitaigorodskii et al.*, 1983; *Agrawal et al.*, 1992]. The observations of reduced ϵ may be caused by the presence of surfactants at the ocean surface damping turbulence, as the Knorr11 campaign experienced high levels of phytoplankton blooms [*Bell et al.*, 2013]. To determine the offset between the observed and scaled profiles, measured ϵ profiles of ASIP were averaged over 200 min time intervals (typically an average of 7 ϵ profiles) and normalized with the LOW (ϵ/ϵ_{LOW}) within the depth of the XLD ($\epsilon_{LOW} = 0.394 \, [\pm \, 0.07] \cdot \epsilon_{LOW}$).

As the LOW does not account for turbulence induced by waves the wave scaling of *Terray et al.* [1996] was also implemented (henceforth T96 scaling). The dissipation rate ϵ_{T96} is scaled by using parameters of the wind-wave field and its vertical structure is divided into three regions. In the uppermost layer, from the surface to a "breaking depth" $z_b = 0.6 \, H_s$, where H_s is the significant wave height, ϵ is assumed to be constant and an order of magnitude larger than predicted by the LOW due to the presence of breaking waves. The energy of this "breaking layer" is dissipated downward to a "transition depth" $z_t = 0.3 \, H_s \frac{\kappa \bar{c}}{u_{*_a}}$, where $\bar{c}$ is the effective wave speed. In this "transition layer" ϵ behaves proportional to z^{-2}. Below the "transition layer" local shear production dominates ϵ induced by breaking waves, and follows the behavior of a shear-driven flow,
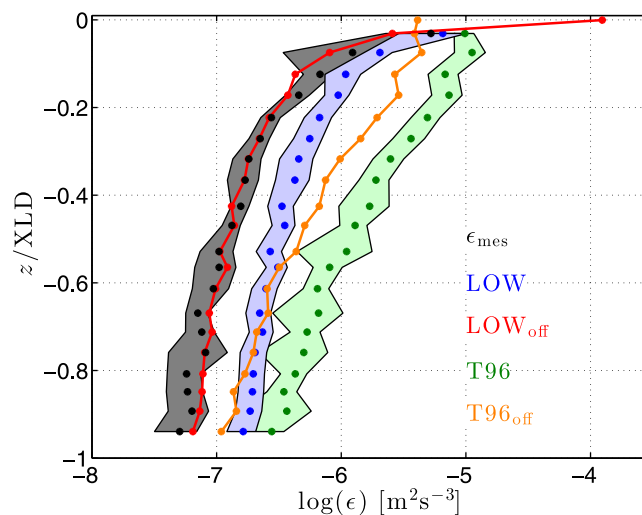
Figure 1. Averaged dissipation profiles, averaged over all ASIP deployments, with their 95% confidence interval (black), and the respective averaged LOW profile (blue) and T96 profiles (green) and their 95% confidence interval. The LOW is fitted to the measurements (multiplied offset of 0.394) and extrapolated to the thickness of the viscous sublayer—the resulting profile is shown in red. The same is done with the T96 scaling (orange). The circles give the averaged values at each normalized depth level—normalized to the mixing layer depth (XLD).

thus proportional to z^{-1}. The ϵ profile can be described as a ratio to the wall layer estimates (equation (13) in *Terray et al.* [1996]):

$$\epsilon_{T96}(z) = \begin{cases} \dfrac{u_*^3 z_t}{\kappa z_b^2} & \text{above } z_b \\[2ex] \dfrac{u_*^3 z_t}{\kappa z^2} & \text{between } z_b \text{ and } z_t \\[2ex] \dfrac{u_*^3}{\kappa z} & \text{below } z_t. \end{cases} \tag{6}$$

During the Knorr11 cruise no "breaking layer" with uniform ϵ was observed contradicting the predictions of T96. The measured values of ϵ are overestimated and the scaled profiles were offset in the same way as for the LOW (Figure 1).

In order to determine ϵ immediately below the air-sea interface, the scaled profiles ϵ_{LOW} and ϵ_{T96} are extrapolated to the thickness of the viscous sublayer, so that $z=z_v$ in (5) and (6 above z_b) following *Lorke and Peeters* [2006]. This thickness is a function of wind speed [*Ward and Donelan*, 2006; *Ward*, 2007] and is inversely proportional to the friction velocity [*Wu*, 1971; *Chriss and Caldwell*, 1984]:

$$z_v = 11 \frac{v}{u_*}. \tag{7}$$

When applying an offset to the scaled ϵ_{T96} profiles (Figure 1), those profiles underestimate the measured ϵ close to the surface, and the extrapolated values of $\epsilon_{0_{T96}}$ at the thickness of the viscous sublayer are consistently smaller than those modeled by the LOW and are often even smaller than the measured ϵ values at 0.5 m depth.

Expressing ϵ_0 with the LOW scaling approach in the SEM allows (3) to be rewritten as:

$$k = A u_* Sc^{-n} \left(\frac{0.394 \, [\pm 0.07]}{11 \, \kappa} \right)^{1/4}, \tag{8}$$

which is a function of u_* rather than ϵ. Therefore, scaling ϵ with the LOW allows to directly compare the SEM with the commonly used wind speed-based parameterizations (over the open ocean wind speed and u_* are closely related as shown by *Edson et al.* [2013]. Here we use the Tropical Ocean Global Atmosphere Coupled Ocean Atmosphere Response Experiment (TOGA COARE) model to relate u_* to u_{10}. The time series of u_* and wind speed are shown in Figure 2.

The parameterization in (8) only includes u_* as a determining parameter and is only valid in situations in which no waves are present, so that the prevailing turbulence is purely shear induced. To take surface waves into account, ϵ_0 in (3) can be expressed with $\epsilon_{0_{T96}}$ providing:

$$k = A Sc^{-n} \left(0.394 \, [\pm 0.007] \frac{u_*^2 \, \overline{c} \, \rho_a \, v}{H_s \, \rho_w} \right)^{1/4} \tag{9}$$

which is a function of u_*, H_s, $\overline{c}$, ρ_a, ρ_w, and v.

2.3. Wave Measurements

The wave measurements during the Knorr cruise were carried out using an ultrasonic altimeter mounted at the bow [*Christensen et al.*, 2013]. To correct for ship motion, the altimeter was combined with an accelerometer. From the obtained time series of sea surface elevation, surface wave spectra were calculated to determine H_s (Figure 2) and the zero-upcrossing period T_0 as described in *Sutherland et al.* [2013].

2.4. Schmidt Number Exponent

Fick's law of diffusion, which states that the flux density J of a tracer being forced by molecular diffusion is proportional to the concentration gradient, can be extended to also account for turbulent transport:

$$J = -(D + K_C) \frac{\partial C}{\partial z}, \tag{10}$$

where D and K_C are the molecular and turbulent diffusion coefficients, respectively. In case of stationarity and homogeneity where no chemical sources or sinks exist, J is directed vertically and constant. Integration of (10) yields:
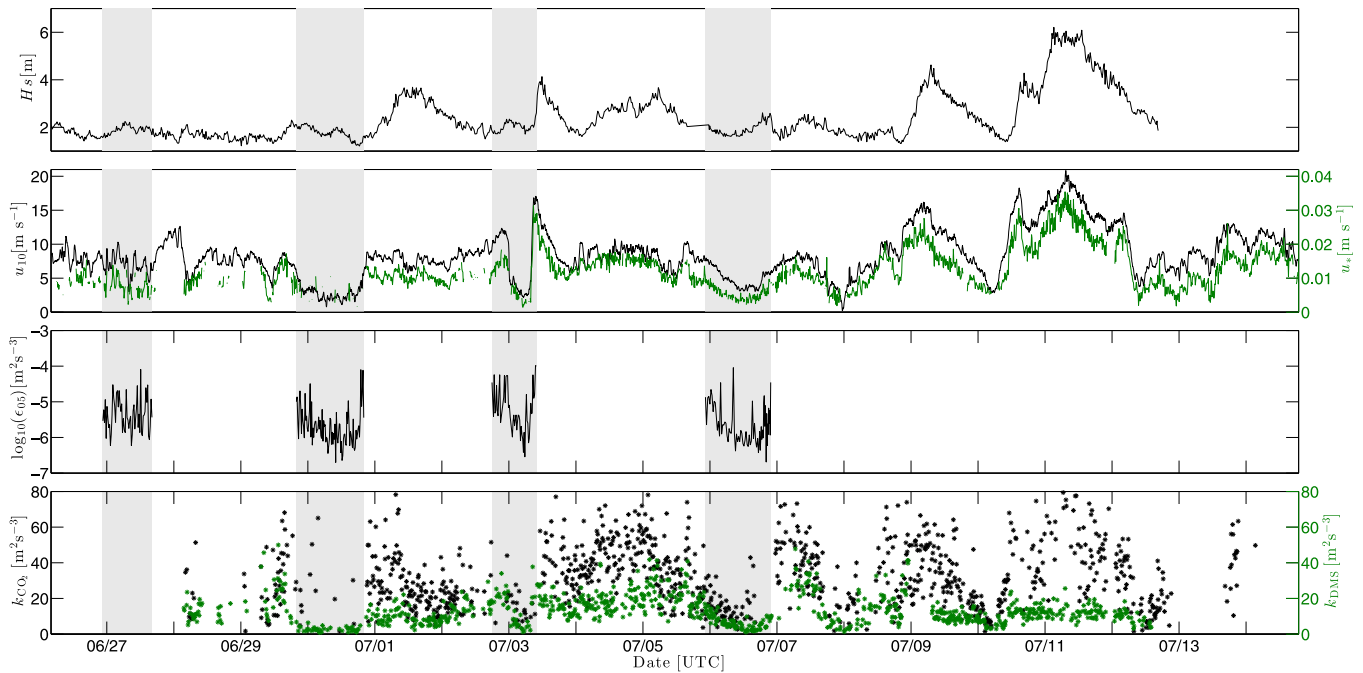
Figure 2. Significant wave height (H_s), wind speed (u_{10}), water side friction velocity (u_*), measured ϵ_{05m}, k_{CO_2}, and k_{DMS} time series of the Knorr11 cruise. The grey shaded areas show the period of ASIP deployments.

$$R = \frac{C(z_\gamma) - C(0)}{J} = \int_0^{z_\gamma} \frac{1}{D + K_C(z)} dz, \tag{11}$$

where R is the resistance which is equal to $1/k$. The profile of K_C close to the air-sea interface depends on the sea surface conditions. For a smooth solid wall, $K_C(z)$ can be described by the Reichardt approach [*Reichardt*, 1951] as $K_C \propto z^3$ close to the surface which changes to a linear relation at larger depth. For a free and wavy surface, the turbulent diffusivity increases with the distance squared ($K_c \propto z^2$) [*Jähne*, 2009]. Integrating (11) using these descriptions of $K_C(z)$ yields the gas transfer velocity k proportional to the Schmidt number:

$$k \propto \begin{cases} Sc^{-2/3} & \text{for a smooth surface} \\ Sc^{-1/2} & \text{for a wavy surface}, \end{cases} \tag{12}$$

where $n = \frac{1}{2}$ and $n = \frac{2}{3}$ give the theoretical limits of the Schmidt number exponent n for a film-covered smooth and a completely wavy ocean surface, respectively [*Deacon*, 1977; *Jähne et al.*, 1987]. Using the dual-tracer method, the change from $n = \frac{2}{3}$ for a film covered surface to $n = \frac{1}{2}$ for a wave-covered surface was verified in tank experiments [*Jähne et al.*, 1985, 1987]. For a Schmidt number of 660, this leads to an increase of k by a factor of 3.

As it is difficult to measure n in the field, most studies concentrate on the relation between ϵ and k and assume $n = \frac{1}{2}$ [*Zappa et al.*, 2007; *Tokoro et al.*, 2008; *Vachon et al.*, 2010; *Gålfalk et al.*, 2013; *Wang et al.*, 2015]. None of the empirical gas transfer models take the transition of the Schmidt number exponent into account. Even though the exact shape of the transition from $n = \frac{2}{3}$ to $n = \frac{1}{2}$ is not known, laboratory studies indicate this transition to occur smoothly and it has been described as a function of mean square slope (total variance of the sea surface slope), the friction velocity, and wind speed [*Krall*, 2013; *Richter and Jähne*, 2011; *Jähne and Haußecker*, 1998]. *Krall* [2013] used the Aeolotron circular flume at the University of Heidelberg to investigate the transition of n based on u_* in the presence of surfactants. For each of the three surfactant conditions (clean surface; medium surfactant coverage with 0.052 mmol/l Triton; and high surfactant coverage with 0.26 mmol/l Triton), they found different relations of $n = f(u_*)$ as shown in Figure 3. For a clean water surface, $n = \frac{2}{3}$ is reached for the lowest u_* and the transition toward $n = \frac{1}{2}$ is the
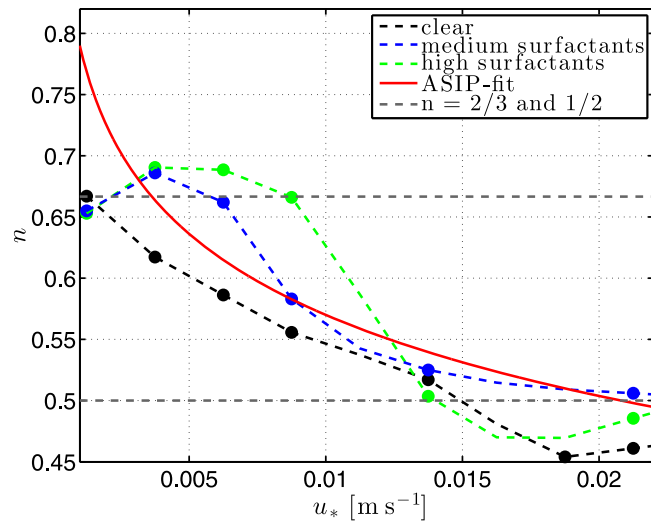
Figure 3. The Schmidt number exponent n as a function of the water side friction velocity u_* based on *Krall* [2013] for high surfactant coverage (0.26 mmol/l Triton in green), medium surfactant coverage (0.052 mmol/l Triton in blue), clean surface (black), and the best fit for $n = f(u_*)$ from the measured k_{DMS} and ϵ in the SEM during Knorr11: $n = -0.22 \cdot \log_{10}(u_*) + 0.13$ (red). The dashed grey-colored lines give the theoretical boundaries of $n = \frac{1}{2}$ and $n = \frac{2}{3}$.

smoothest. For higher surfactant coverage, the relation becomes steeper and the onset is shifted to higher u_* values.

The least-square method was used to calculate $n = f(u_*)$ from our observations. This was performed separately for k_{DMS} and k_{CO_2} using equation (3). As the SEM describes the physical mechanism occurring at the air-sea interface, the values of ϵ being extrapolated to z_v assuming the LOW are used to find the best fit. These $\epsilon_{0_{LOW}}$ do not rely on the actually measured ϵ but on u_* based on in situ momentum flux measurements, which allows us to take all combined measurements of k and u_* from the Knorr11 and the SOAP cruises into account. The best fits are determined with respect to the best combination in the proportionality coefficient A and $n = f(u_*)$ in the SEM.
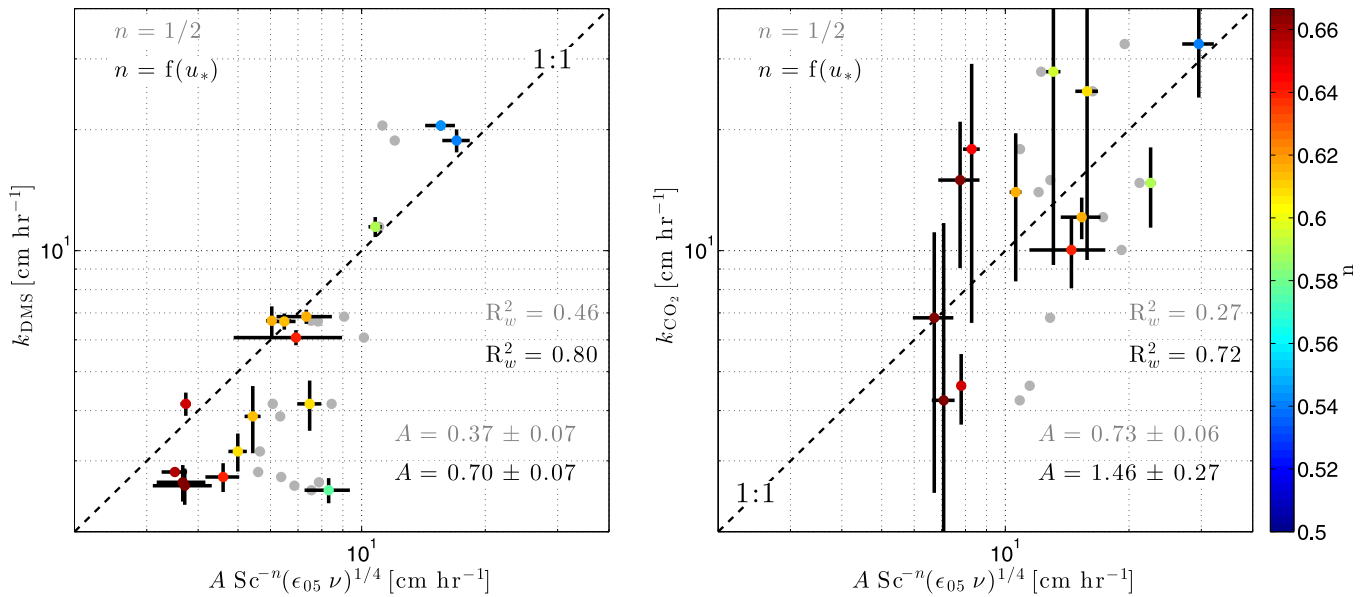
Following this assumption, a function $n = -0.22 \cdot \log_{10}(u_*) + 0.13$ is determined based on k_{DMS}, which is associated with an $A = 0.20$. A similar fit was determined based on the k_{CO_2} observations. As the fit based on observations of k_{DMS} describes the relation between k and the SEM better (RMSD $= \pm 7.18$ cm h^{-1}) than the one based on observations of k_{CO_2} (RMSD $= \pm 9.03$ cm h^{-1}), in the following this fit is chosen to describe the transition of n for both gases.

When calculating $n = f(u_*)$ from our observations using the least-square method, we find a function that follows closest the medium surfactant case of *Krall* [2013] (Figure 3). It is reasonable to assume that there may have been biological surfactants present, given the high levels of chlorophyll observed during the Knorr11 cruise [*Bell et al.*, 2013].

3. Results and Discussion

3.1. Small-Eddy Model

The SEM for data averaged over 200 min intervals describes 46% of the variability in k_{DMS} when applying constant $n = \frac{1}{2}$, as it was assumed by previous studies [e.g., *Zappa et al.*, 2007] (Figure 4a in grey). The performance of the SEM can be significantly improved, when applying a variable $n = f(u_*)$, which then describes 80% of the variability in k_{DMS} (Figure 4a in color).

The measured k_{CO_2} is much more variable than the k_{DMS}, especially for lower wind speeds. This high variability leads to a lower correlation, where the weighted coefficient of determination is, $R_w^2 = 0.72$ for a variable $n = f(u_*)$ and $R_w^2 = 0.27$ for $n = \frac{1}{2}$. The weighted correlation coefficient is given by $R_w^2 = 1 - \frac{\sum_i (y_i - x_i)^2 / \sigma_i^2}{\sum_i (y_i - \bar{y})^2 / \sigma_i^2}$ and takes the relative error σ_i of each data point i into account, where y and x are the observed and predicted data, respectively.

Until now, we have looked at the relation based on ϵ measured in the uppermost 0.5 m of the ocean. However, the SEM is defined for an ϵ_0 measured directly at the air-sea interface. To account for this, the measured profiles of ϵ are extrapolated to the depth of the viscous sublayer z_v, using the LOW and the T96 scaling (Figure 1). Figure 5 shows the same setup as Figure 4 with ϵ extrapolated to z_v (equations (8) and (9)).

The SEM holds well for this extrapolated data for both k_{DMS} ($R_{w_{LOW}}^2 = 0.85$ and $R_{w_{T96}}^2 = 0.78$) and k_{CO_2} ($R_{w_{LOW}}^2 = 0.69$ and $R_{w_{T96}}^2 = 0.67$) based on the LOW and the wave induced turbulence T96 scaling all for a

Figure 4. Measured (left) k_{DMS} and (right) k_{CO_2} versus the prediction of the SEM based on measured ϵ taken within the uppermost 0.5 m of the ocean averaged over 200 min intervals in log-log space. The color code represents $n = f(u_*)$, the errors bars show the std-error. The grey data in the background represent the same calculations based on a constant Schmidt number exponent of $n = \frac{1}{2}$. (Note that applying $n = f(u_*)$ shifts the data points parallel to the x axis.) The dashed line shows the 1:1 relation between measured k and the SEM. The proportionality coefficient A is determined using a weighted least-square method and the R_w^2 values is weighted with the relative errors of the averaged measurements. For the analysis all temporal bins, which hold only one data point and those with a standard deviation higher than 8 times the averaged standard deviation were excluded.

variable n. These R_w^2 values are close to the ones determined for the analysis based on the measured ϵ_{05m} in Figure 4 (an increase of 6% and decrease of 3% for $R_{w_{LOW}}$ and $R_{w_{T96}}$, respectively, for k_{DMS} and a decrease of 4% and 7% for $R_{w_{LOW}}$ and $R_{w_{T96}}$, respectively, for k_{CO_2}). This indicates that both the LOW and the T96 scaling are appropriate methods for parameterizing k.
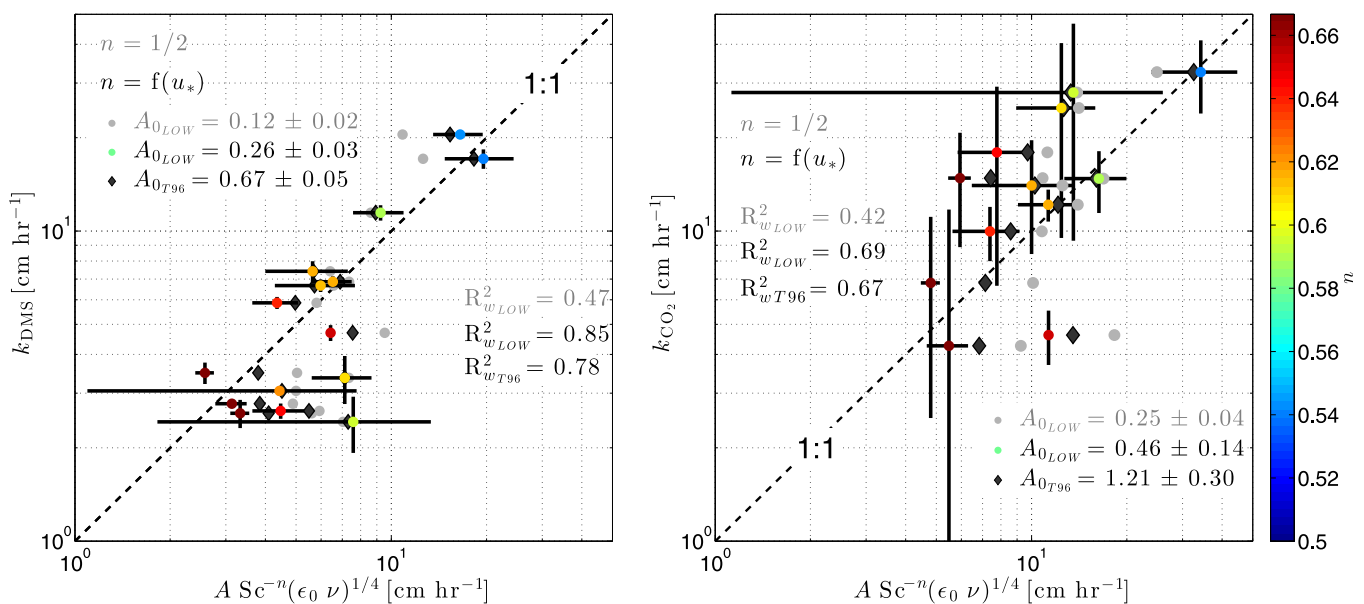

Figure 5. Same as in Figure 4 except with ϵ extrapolated to the surface using LOW scaling based on the measured u_* values (colored data points) and using the T96 scaling (black diamonds).

3.2. Relating the Gas Transfer Velocity to Modeled Dissipation Estimates

Figure 6 shows the prediction of the SEM based on u_* (equation (8)) and the scaled wave-induced turbulence (equation (9)) for the complete Knorr11 data including the periods for which ASIP was not deployed (Figure 2). For both scaling approaches, it shows a linear relation for k_{DMS} at low and medium wind speeds (Figure 6a). Only at high wind speeds, which correspond to the last station of the Knorr11 cruise, k_{DMS} significantly deviates from this linear relation, which has been discussed by *Bell et al.* [2013]. They speculate that variations in surfactants and/or wind/wave interactions are causing this deviation. When excluding this last station from the analysis, the SEM explains 94% of the variability based on the LOW and 91% based on the T96 scaling in k_{DMS}. Therefore, the SEM explains a large part of the variability in k_{DMS} for low and medium wind speeds.

For high wind speeds, there exist no direct measurements of ϵ during the Knorr11 cruise because the recovery of ASIP after the storm failed. A reduction in ϵ during these high wind speeds could explain the discrepancy between the predicted and the measured k_{DMS}. The SEM successfully predicted k_{CO_2} at high wind speeds (Figure 6b). The different behavior of k_{DMS} and k_{CO_2} in high winds could be explained by a reduction in ϵ with a simultaneous increase in bubble-mediated transfer, which is expected to be relevant for CO_2 but not for DMS [*Bell*, 2015; *Gemmrich*, 2012]. Figure 6b shows the same analysis for k_{CO_2} for which the SEM explains 27% and 25% of the variability based on the LOW and T96 scaling, respectively. Highest variability of the measured k_{CO_2} occurs at low wind speeds.

The prediction of the SEM based on different scaling approaches (excluding and including surface waves) yield similar strong results for k_{DMS} and k_{CO_2} with T96 explaining nearly as much of the variability as the LOW.

Having consistent measurements of u_*, k_{DMS}, and k_{CO_2}, the same analysis based on $\epsilon_{0_{LOW}}$ is applied to k measured in the Pacific during the SOAP cruise. Taking the same relation determined for the North Atlantic and applying them on the k_{DMS} and k_{CO_2} measurements in the Pacific explains 76% of the variability for k_{DMS} and 98% for k_{CO_2} (Figure 7).

When inserting the proportionality coefficients $A_{0_{LOW}}$ found for $\epsilon_{0_{LOW}}$ in the North Atlantic (Figure 6) and for the Pacific (Figure 7) into equation (8), k can be parameterized by:

$$k_{CO_2} = 0.224 \, [\pm 0.06] \, u_* \cdot Sc^{-(0.13 - 0.22 \cdot \log_{10}(u_*))}$$

(13)

(with $A = 0.39 \, [\pm 0.02]$ for Knorr11 and $A = 0.43 \, [\pm 0.06]$ for SOAP)
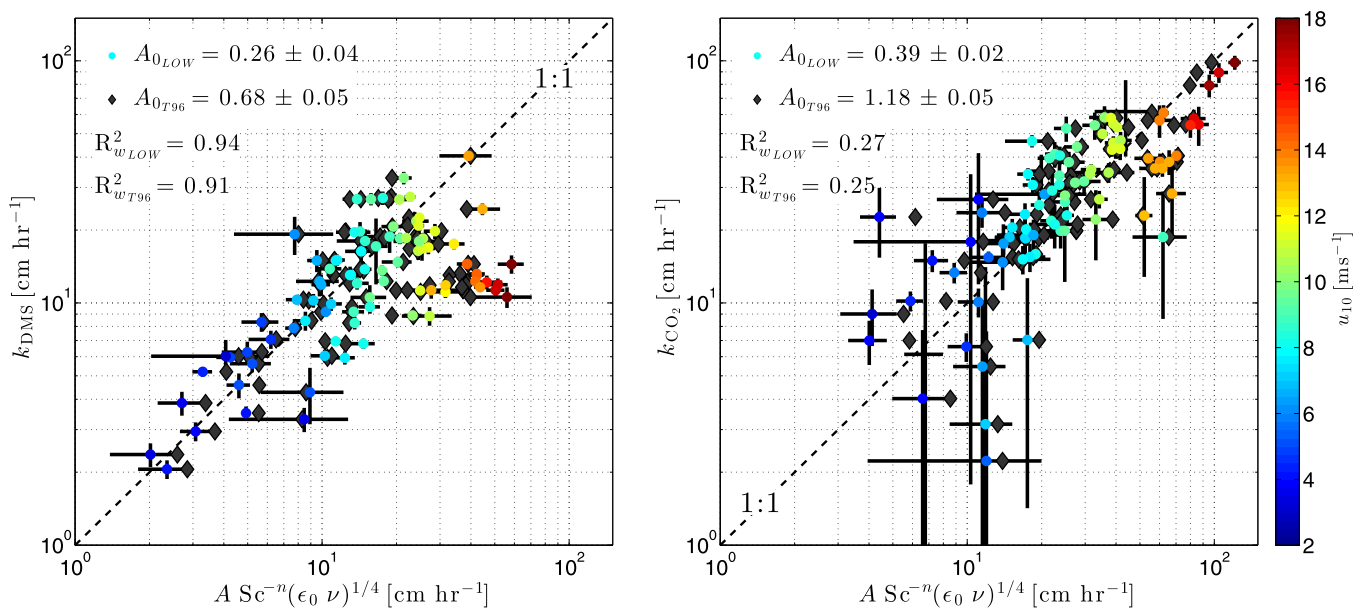

Figure 6. Same as Figure 4 except with ϵ extrapolated to the surface using LOW scaling based on the measured u_* values (colored data points) and using the T96 scaling (black diamonds) applied to the complete Knorr11 data set. The R_w^2 value for k_{DMS} excludes the measurements of k made during station 191.
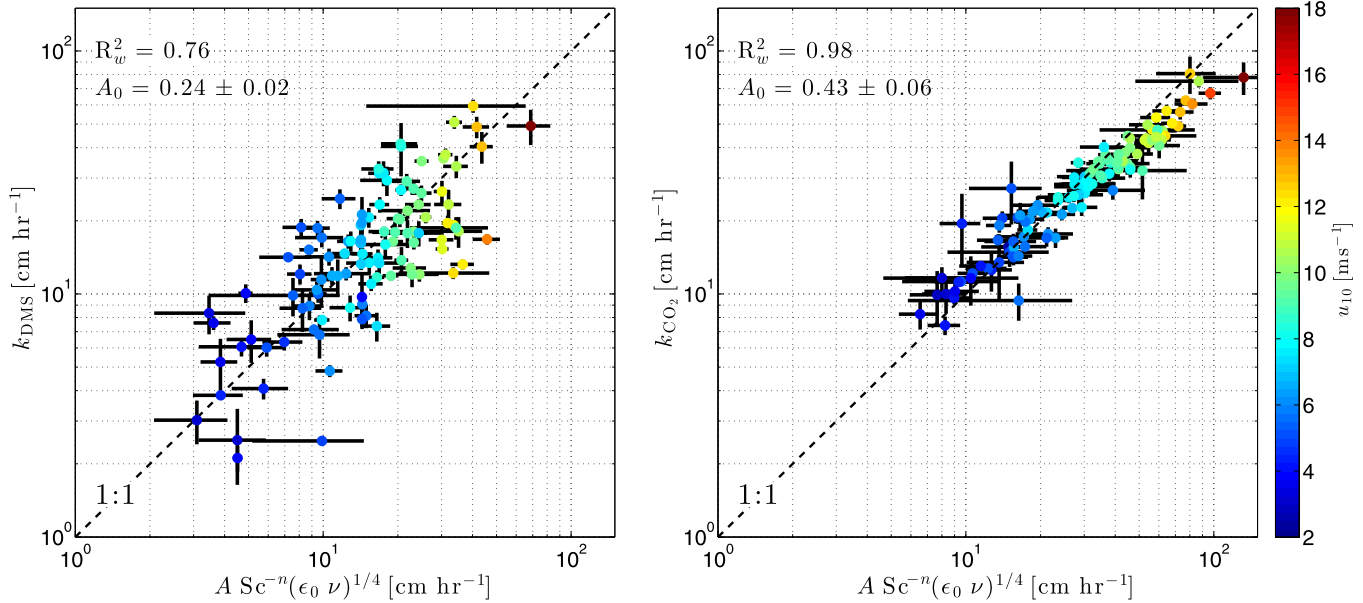
Figure 7. Same as Figure 4 except with ϵ extrapolated to the surface using LOW scaling based on the measured u_* values for the complete SOAP data without showing results based on the T96 scaling as it was not calculated for the SOAP cruise.

$$k_{\text{DMS}} = 0.137 \left[\pm 0.04\right] u_* \cdot \text{Sc}^{-(0.13 - 0.22 \cdot \log_{10}(u_*))}$$

(14)

(with $A = 0.26 \left[\pm 0.04\right]$ for Knorr11 and $A = 0.24 \left[\pm 0.02\right]$ for SOAP).

Using the LOW to determine these parameterizations assumes the ocean to be purely shear driven, therefore ignoring any wave-enhanced turbulence near the surface. Different scaling approaches, which suggest a deviation from the LOW with ϵ being proportional to z^{-2} to z^{-4} [*Gargett*, 1989; *Craig and Banner*, 1994; *Terray et al.*, 1996; *Sutherland and Melville*, 2015], change the magnitude of the extrapolated ϵ_0 and thus the proportionality coefficient A. However, for T96, it is shown that the performance of the SEM is not changed significantly. When inserting the proportionality coefficients A for $\epsilon_{0_{T96}}$ in the North Atlantic (Figure 6 and equation (9)), k can be parameterized by:

$$k_{\text{CO}_2} = 0.89 \left[\pm 0.20\right] \text{Sc}^{-n} \left(\frac{u_*^2 \, \bar{c} \, \rho_a \, \nu}{H_s \, \rho_w} \right)^{1/4}$$

(15)

(with $A = 1.18 \left[\pm 0.05\right]$ for Knorr11)

$$k_{\text{DMS}} = 0.51 \left[\pm 0.13\right] \text{Sc}^{-n} \left(\frac{u_*^2 \, \bar{c} \, \rho_a \, \nu}{H_s \, \rho_w} \right)^{1/4}$$

(16)

(with $A = 0.68 \left[\pm 0.05\right]$ for Knorr11).

Neither of the scaling attempts perfectly describes the measured ϵ profiles during Knorr11. The profiles modeled by the T96, scaled with a depth dependency of ϵ_{T96} over-predict the magnitude of the measured ϵ profiles even further than the LOW (Figure 1). To overcome this over-prediction, an offset was applied. At the depth of the viscous sublayer, above the "breaking" depth z_b, the uniform ϵ_{T96} falls below the values predicted by the LOW. Further investigations on scaling ϵ close to the air-sea interface are desirable to accurately describe ϵ_0. This scaling could then be used to extrapolate ϵ in the SEM to z_ν and to obtain a more accurate and more universally applicable parameterization of k.

The performance of both scaling approaches within the SEM was equally feasible (similar R_w^2 values for both scaling approaches in Figure 5). The LOW, which is only applicable when no waves occur, offers a straightforward opportunity to compare the commonly used empirical wind speed parameterizations with the SEM using equations (13) and (14) (Figure 8). This attempt is worthwhile to address as wave measurements
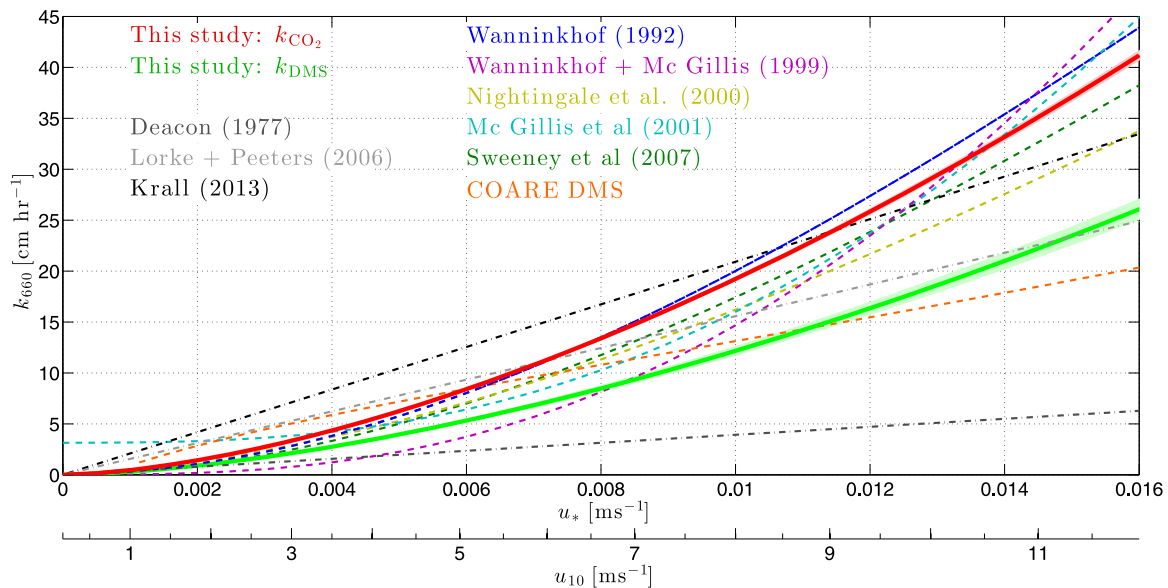
Figure 8. A selection of wind speed-based (dashed lines) and friction velocity (dashed-dotted lines) gas transfer velocity parameterizations are compared to the turbulence-based parameterization determined in this study (solid lines) for k_{DMS} (green) and k_{CO_2} (red). These lines do not implicate any direct measurements but are based on idealized water side friction velocity u_* using the $k = f(u_*)$ relations determined in this study in equations (13) and (14). The range (shaded area) of these relations is caused by the different proportionality coefficients A for the North Atlantic and the Pacific. Note that u_* and u_{10} are not related linearly with each other.

would be necessary for the T96 scaling, which are not achievable for every measurement campaign. Note that the wave measurements during the Knorr11 campaign provided only 1-D wave spectra, this does not allow to account for the full complexity of the wave field, e.g., alignment of swell and wind sea or directional spread of the wave spectrum.

The function derived for k_{CO_2} based on the LOW falls between the estimates of *Wanninkhof* [1992] and *Sweeney et al.* [2007] (Figure 8). The latter parameterization is an update of the first based on a revision of the ^{14}C data. Our function for k_{DMS} based on the LOW lies in the lower range of the conventional wind-based parameterizations and is in the range of the results of the COARE model for DMS.

For a completely smooth water surface ($n = \frac{2}{3}$), *Deacon* [1977] derived k based on u_* using the turbulent diffusion model (Table 1), which can be interpreted as a lower boundary for the wind driven gas transfer. Our $k = f(u_*)$ relation results in higher values of k for both gases and comes close to Deacon's theoretical relation only for the lowest wind speeds (Figure 8). *Krall* [2013] empirically fitted an upper boundary to their measurements for surfactant-free conditions using $n = \frac{1}{2}$. Our k_{DMS} relation based on the LOW falls within these boundaries showing the transition from a completely smooth to wavy ocean surface. Our relation for k_{CO_2} exceeds the empirical upper boundary of *Krall* [2013].

Table 1. Wind Speed u_{10} and Friction Velocity u_* Based Parameterizations Used in Figure 8 for Comparison to the Relation Determined in This Study

Wanninkhof [1992]	$k_{660} = 0.31\, u_{10}^2$
Wanninkhof and McGillis [1999]	$k_{660} = 0.0283\, u_{10}^3$
Nightingale et al. [2000]	$k_{600} = 0.222\, u_{10}^2 + 0.333\, u_{10}$
McGillis et al. [2001]	$k_{600} = 3.3 + 0.026\, u_{10}^3$
McGillis et al. [2004]	$k_{600} = 8.2 + 0.014\, u_{10}^3$
Sweeney et al. [2007]	$k_{660} = 0.27\, u_{10}^2$
Deacon [1977]	$k = 0.0826 \cdot Sc^{-2/3} u_*$
Lorke and Peeters [2006]	$k = 0.1111 \cdot Sc^{-1/2} u_*$
Krall [2013]	$k = 0.1493 \cdot Sc^{-1/2} u_*$
This study for CO$_2$	$k = 0.224\ [\pm 0.06] \cdot Sc^{-n} u_*$
This study for DMS	$k = 0.137\ [\pm 0.04] \cdot Sc^{-n} u_*$
	where $n = 0.13 - 0.22 \cdot log_{10}(u_*)$

3.3. Proportionality Coefficient A

The proportionality between both sides of the SEM (equation (3)) is expressed by the coefficient A, which is determined through data regression. At the measurement depth of 0.5 m, A is determined to be 0.70 [± 0.07] for k_{DMS} when using a variable $n = f(u_*)$. When using $n = \frac{1}{2}$ for k_{DMS}, A is determined to be 0.37 [± 0.07], which is similar to the values found in a wide range of field studies by *Zappa et al.* [2007] ($A = 0.419$ [± 0.130]) and also for large lakes ($A = 0.44$ [± 0.01]) as well as for small lakes

Table 2. Proportionality Coefficients A, Measurement Depth, and the Used Schmidt Number Exponent n Found in the Literature and Determined in This Study

	A	Depth (m)	n
Present study—DMS	0.70 ± 0.07	0–0.5	$n=f(u_*)$
–CO_2	1.46 ± 0.27	0–0.5	$n=f(u_*)$
–DMS	0.26 ± 0.04 (Knorr-LOW)	z_v	$n=f(u_*)$
	0.68 ± 0.05 (Knorr-T96)	z_v	$n=f(u_*)$
	0.24 ± 0.02 (SOAP-LOW)	z_v	$n=f(u_*)$
–CO_2	0.39 ± 0.02 (Knorr-LOW)	z_v	$n=f(u_*)$
	1.18 ± 0.05 (Knorr-T96)	z_v	$n=f(u_*)$
	0.43 ± 0.06 (SOAP-LOW)	z_v	$n=f(u_*)$
–DMS	0.37 ± 0.07	0–0.5	1/2
–CO_2	0.73 ± 0.06	0–0.5	1/2
–DMS	0.12 ± 0.02 (LOW)	z_v	1/2
	0.30 ± 0.01 (T96)	z_v	1/2
–CO_2	0.25 ± 0.04 (LOW)	z_v	1/2
	0.59 ± 0.10 (T96)	z_v	1/2
Zappa et al. [2007]	0.419 ± 0.130	Few cm to 3 m	1/2
Tokoro et al. [2008]	0.18 ± 0.04	Scaled to 0.86 m	1/2
Vachon et al. [2010]	0.44 ± 0.01	0.1	1/2
—large lakes			
—small lakes	0.39 ± 0.02	0.1	1/2
Gålfalk et al. [2013]	0.42	0.3	1/2
Wang et al. [2015]	0.08–0.34	0.025	1/2
	0.1–0.43	0.1	1/2

($A = 0.39$ [± 0.02]) observed by *Vachon et al.* [2010]. Thus, the proportionality for k_{DMS} between both sides of the SEM found in the open ocean is similar to the ones found in previous studies when using the same assumptions (summarized values of A in Table 2).

As the measured k_{CO_2} are greater than the measured k_{DMS}, the values of A have to be proportionally higher for k_{DMS}. The differences in the values between k_{CO_2} and k_{DMS} might be driven by wave/bubble effects. Breaking waves and bubbles are suggested to enhance the transfer of lower solubility gases like CO_2 relative to higher solubility gases like DMS. The coefficient A based on a constant n for k_{CO_2} is lower ($A = 0.73$ [± 0.06]) than for a variable $n=f(u_*)$ ($A = 1.46$ [± 0.27]). These values of A are significantly higher than those found in the literature.

As pointed out before, the T96 scaling with applied offset predicts lower values of ϵ_0 than the LOW. The different magnitude of ϵ_0 from both scaling approaches is reflected in different values of the constant A_0, which has to balance the different ϵ_0 (Figure 4). The values of $A_{0_{T96}}$ are higher than the $A_{0_{LOW}}$ for both k_{DMS} ($A_{0_{T96}} = 0.67$ [± 0.05] and $A_{0_{LOW}} = 0.26$ [± 0.03]) and k_{CO_2} ($A_{0_{T96}} = 1.21$ [± 0.30] and $A_{0_{LOW}} = 0.46$ [± 0.14]).

For the extrapolated $\epsilon_{0_{LOW}}$, $A_{0_{LOW}}$ was predetermined for k_{DMS} to be $A_0 = 0.20$, when using the least-square fitting to assess $n=f(u_*)$ (section 2.4). This approach was based on the complete Knorr11 and SOAP data. As
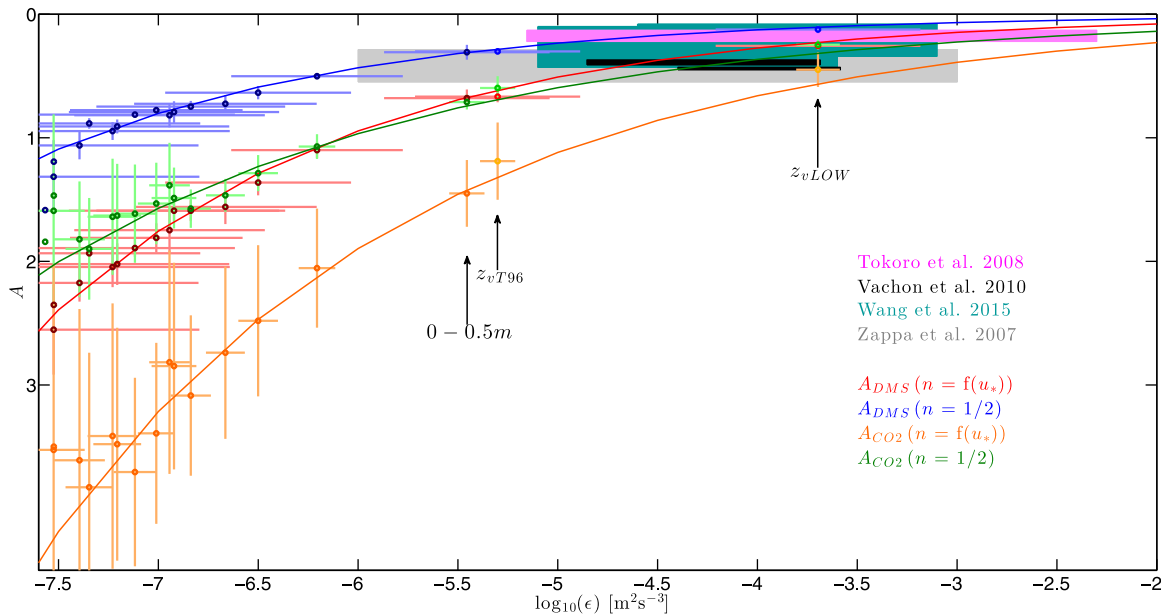

Figure 9. The proportionality coefficient A versus the dissipation rate of TKE based on k_{DMS} (for $n=f(u_*)$ in red and $n=\frac{1}{2}$ in blue) and k_{CO_2} (for $n=f(u_*)$ in orange and $n=\frac{1}{2}$ in green) based on ASIP measurements during the Knorr11 cruise. The circles give the relation calculated for 0.5 m depth intervals of the measured ϵ profiles and the lines show the best fitted functions. The relations found for the viscous sublayer for both the LOW scaling (z_{vLOW}) and the T96 scaling (z_{vT96}) as well as the uppermost 0.5 m are highlighted. The Knorr11 data are shown together with data from the literature.

Table 3. Determined Coefficients to Describe the Dependency of the Proportionality Coefficient A of the SEM on ϵ: $A=\beta_\epsilon z^{\gamma_\epsilon}$ $A=\beta_\epsilon \epsilon^{\gamma_\epsilon}$

	β_ϵ	γ_ϵ
k_{CO_2} and $n=\frac{1}{2}$	-0.211	0.052
k_{CO_2} and $n=f(u_*)$	-0.229	0.080
k_{DMS} and $n=\frac{1}{2}$	-0.267	0.011
k_{DMS} and $n=f(u_*)$	-0.269	0.023

the extrapolated $\epsilon_{0_{LOW}}$ based on the ASIP measurements only shows a small segment of this complete data in relatively low wind speeds, it is not surprising, that $A_{0_{LOW}} = 0.26 [\pm 0.03]$ does not agree perfectly with this predetermined value.

When taking the complete Knorr11 data into account, A_0 changes within the range of error for the SEM based on both scaling approaches, from $A_{0_{LOW}} = 0.46 [\pm 0.14]$ and $A_{0_{T96}} = 1.21 [\pm 0.30]$ for the extrapolated ASIP ϵ_0 to $A_{0_{LOW}} = 0.39 [\pm 0.02]$ and $A_{0_{T96}} = 1.18 [\pm 0.05]$ for the complete Knorr11 data for k_{CO_2} and from $A_{0_{LOW}} = 0.26 [\pm 0.03]$ and $A_{0_{T96}} = 0.67 [\pm 0.05]$ the extrapolated ASIP ϵ_0 to $A_{0_{LOW}} = 0.26 [\pm 0.04]$ and $A_{0_{T96}} = 0.68 [\pm 0.05]$ the complete Knorr11 data for DMS. The values obtained for A in the Pacific based on the LOW scaling are for both gases the same (within the range of error) than found in the North Atlantic.

The most significant difference between the SEM based on the measured ϵ at a depth of 0.5 m and the one based on the extrapolated ϵ_0 is the change in the proportionality constant A for both gases as it has to balance the change of ϵ toward the air-sea interface. For the LOW, these extrapolated $\epsilon_{0_{LOW}}$ are higher than those measured at 0.5 m depth, so that A has to decrease toward the surface. As the offset T96 scaling predicts values in a similar range than the measured ϵ close to the ocean surface, likewise the extrapolated $\epsilon_{0_{T96}}$ are similar to those measured at 0.5 m depth and thus A_0 has to stay in the same range than A found in 0.5 m depth. The values of A found for the extrapolated ASIP $\epsilon_{0_{LOW}}$ show lower values ($A_{0_{LOW}} = 0.12 [\pm 0.02]$ for k_{DMS} and $A_{0_{LOW}} = 0.25 [\pm 0.04]$ for k_{CO_2} for constant $n=\frac{1}{2}$) than for ϵ measured at 0.5 m. These values of $A_{0_{LOW}}$ for the commonly used $n=\frac{1}{2}$ are closer to those observed by *Wang et al.* [2015] ($0.08 \leq A \leq 0.34$), measured at 0.25 cm depth, than the A found for the same setting within the layer down to 0.5 m. This shows the depth dependency of A, which makes a comparison with previous studies more difficult since for each study ϵ was measured at different depths. The ASIP profiles provide ϵ measurements covering a wide range of water depths. This offers the great opportunity to investigate the depth dependency of the proportionality "constant" A. The same analysis as carried out for the uppermost 0.5 m is implemented for depth intervals of 0.5 m. The values for A in these depth intervals are presented against the prevailing turbulence in Figure 9.

Despite showing A as a function of ϵ, there is also a clear depth dependency. The coefficient A balances the $k-\epsilon$ relation and consequently follows the strong depth dependency of ϵ. However, for the comparison of our results to previously published values of A, it is clearer to use A based on $\epsilon=f(z)$. This approach offers the ability to relate A and ϵ without information about the depth (Figure 9).

When ignoring the measurement depth and only concentrating on the prevailing turbulences, we can formulate $A=\beta_\epsilon \epsilon^{\gamma_\epsilon}$ with β_ϵ and γ_ϵ listed in Table 3. This function gives a range of values for A based on measurements of ϵ at different levels of turbulences. Therefore, a known value of ϵ gives the proportionality in the SEM which then predicts the prevailing k.

When comparing these functions to the literature (where $n=\frac{1}{2}$), good agreement for both k_{DMS} and k_{CO_2} is found. As the functions fit well with the $A-\epsilon$ relations found in estuaries and coastal oceans they offer a good opportunity to predict $A=f(\epsilon(z))$. The values of A for $n=f(u_*)$ are, as expected, higher than those found in the literature.

To avoid using ϵ as a proxy for the depth dependency of A, we normalized the measured u_* to 0.01 m s^{-1} so that $A=f(z, u_{*norm})$, and thus get a depth dependency of $A=\beta_z z^{\gamma_z}$ with β_z and γ_z for both scaling approaches as listed in Table 4.

Table 4. Same as Table 3 but for A as a Function of Depth Using a Normalized u_* to 0.01 m s^{-1}: $A=\beta_\epsilon \epsilon^{\gamma_\epsilon}$

	β_z	γ_z
k_{CO_2} and $n=\frac{1}{2}$	0.272	0.897
k_{CO_2} and $n=f(u_*)$	0.300	1.735
k_{DMS} and $n=\frac{1}{2}$	0.146	0.495
k_{DMS} and $n=f(u_*)$	0.145	1.089

4. Conclusion

Various studies on gas exchange across the air-sea interface, including a variety of methods and techniques ranging from theoretical approaches, laboratory studies, and field campaigns in lakes, coastal areas, and estuaries, have verified the dissipation rate of turbulent kinetic energy ϵ to be a good

predictor for k using the small-eddy model (SEM) [*Lorke and Peeters*, 2006; *Asher and Pankow*, 1986; *Moog and Jirka*, 1999; *Zappa et al.*, 2007; *Tokoro et al.*, 2008; *Vachon et al.*, 2010]. In this paper, we have used eddy covariance DMS and CO_2 gas transfer measurements and observations from the Air-Sea Interaction Profiler (ASIP) to confirm that this theoretical model holds well for ϵ measured at 0.5 m depth in the open ocean.

It was shown that the performance of the SEM can be significantly improved by using a varying Schmidt number exponent n, which is determined as a function of u_*, instead of the frequently used constant of $n = \frac{1}{2}$. When applying the same assumption that $n = \frac{1}{2}$, as in former studies, the SEM explains 46% of the variability in k_{DMS} and 27% of the variability in k_{CO_2}. Applying $n = f(u_*)$ improves the predictability of the SEM to 80% for k_{DMS} and 72% for k_{CO_2}. This $n = f(u_*)$ changes the SEM in a similar way to the approach of *Wang et al.* [2015], who scale the proportionality coefficient with $A \propto log(\epsilon)$. In both cases, the expression is shifted toward lower values for low ϵ and toward higher values for high ϵ.

We tested the two cases of "no waves" (law of the wall—LOW) and "wave-induced turbulences" (scaling proposed by *Terray et al.* [1996] –T96) to extrapolate our measurements of ϵ to the viscous sublayer z_v. For both cases, we found that our basic analysis holds well, but with different set of model constants. The SEM based on both scaling approaches yields good results for both gases ($R^2_{w_{LOW}} = 0.85$ and $R^2_{w_{T96}} = 0.78$ for k_{DMS} and $R^2_{w_{LOW}} = 0.69$ and $R^2_{w_{T96}} = 0.67$ for k_{CO_2}). The main difference between the scaling approaches is the different profile behavior. When fitting the modeled ϵ profiles to the measured ones, the uniform values of ϵ_{T96} in the "breaking layer", tends to model lower values of ϵ_0 for the viscous sublayer than the LOW. These differences toward the LOW in the magnitude of extrapolated ϵ_0 are reflected in the difference in the proportionality coefficient A for the SEM based on the different scaling approaches. A is determined for a certain ϵ for a measured k according to the SEM. Moving away from the surface, A has to increase in order to obtain the same k because ϵ decreases.

Reliable wave measurements are not conducted during every field experiment, therefore the feasible results of the SEM based on the LOW are promising. Using the LOW to model ϵ_0 enables the simplification of the SEM and a physically based parameterization that solely depends on the water side friction velocity u_* in equations (13) and (14). This relation, which holds not only in the North Atlantic but also in the Pacific Ocean, allows for a validation of the commonly used wind speed parameterization, where the LOW provides a good enough parameterization. At that, our relation follows closest the parameterization of *Sweeney et al.* [2007]. As measuring ϵ_0 directly at the air-sea interface is complicated and none of the proposed scaling approaches could scale the ϵ profiles during Knorr11 perfectly, the usage of parameterizations based on u_* measurements appears to be a reliable alternative for low to intermediate wind speeds.

For the SEM, there exists a range of different values of proportionality coefficients A in literature. These different values of A are based on measurements at various depths and feature a broad range of magnitudes for ϵ. The profiling ability of ASIP was exploited to evaluate the dependency of A on ϵ, which make a comparison between the different studies possible. The determined functions of $A = f(\epsilon)$ cover the published values of A from *Zappa et al.* [2007], *Wang et al.* [2015], *Tokoro et al.* [2008], and *Vachon et al.* [2010]. Normalizing u_* to 0.01 m s^{-1} let us formulate an applicable A-z relation (Table 4), which mirrors A to be a function of measurement depth. This function could help to overcome the uncertainty in A which has limited the application of the SEM to estimate k.

References

Agrawal, Y. C., E. A. Terray, M. A. Donelan, P. A. Hwang, and A. J. Williams III (1992), Enhanced dissipation of kinetic energy beneath surface waves, *Nature*, *359*, 219–220.

Asher, W., and J. F. Pankow (1986), The interaction of mechanically generated turbulence and interfacial films with a liquid phase controlled gas/liquid transport process, *Tellus, Ser. B 38*,(5), 305–318.

Bakker, D. C. E., et al. (2016), A multi-decade record of high-quality fCO$_2$ data in version 3 of the Surface Ocean CO$_2$ Atlas (SOCAT), *Earth Syst. Sci. Data*, *8*, 383–413, doi:10.5194/essd-8-383-2016.

Bell, T. G. (2015), Quantifying the effect of bubbles upon air-sea gas exchange, paper presented at SOLAS Open Science Conference 2015, Kiel, Germany.

Bell, T. G., W. De Bruyn, S. D. Miller, B. Ward, K. H. Christensen, and E. S. Saltzman (2013), Air/sea dimethylsulfide (DMS) gas transfer in the North Atlantic: Evidence for limited interfacial gas exchange at high wind speed, *Atmos. Chem. Phys.*, *13*, 11,073–11,087, doi:10.5194/acp-13-11073-2013.

Bell, T. G., W. De Bruyn, C. A. Marandino, S. D. Miller, C. S. Law, M. J. Smith, and E. S. Saltzman (2015), Dimethylsulfide gas transfer coefficients from algal blooms in the southern ocean, *Atmos. Chem. Phys.*, *15*(4), 1783–1794, doi:10.5194/acp-15-1783-2015.

Brainerd, K. E., and M. C. Gregg (1995), Surface mixed and mixing layer depths, *Deep Sea Res., Part I*, *42*(9), 1521–1543.

Chriss, T. M., and D. R. Caldwell (1984), Universal similarity and the thickness of the viscous sublayer at the ocean floor, *J. Geophys. Res.*, *89*, 6403–6414.

Christensen, K. H., J. Röhr, B. Ward, I. Fer, G. Broström, Ø. Sætra, and Ø. Breivik (2013), Surface wave measurements using ship mounted ultrasonic altimeter, *Methods Oceanogr.*, *6*, 1–15, doi:10.1016/j.mio.2013.07.002.

Craig, P. D., and M. L. Banner (1994), Modeling wave-enhanced turbulence in the ocean surface layer, *J. Phys. Oceanogr.*, *24*, 2546–2559.

Danckwerts, P. V. (1951), Significance of liquid film coefficients in gas absorption, *Ind. Eng. Chem.*, *43*(6), 1460–1467, doi:10.1021/ie50498a055.

Davies, J. T. (1972), *Turbulence Phenomena*, Academic Press, New York.

Deacon, E. L. (1977), Gas transfer to and across an air-water interface, *Tellus*, *29*(4), 363–374.

Edson, J. B., V. Jampana, R. A. Weller, S. P. Bigorre, A. J. Plueddemann, C. W. Fairall, S. D. Miller, L. Mahrt, D. Vickers, and H. Hersbach (2013), On the exchange of momentum over the open ocean, *J. Phys. Oceanogr.*, *43*, 1589–2590.

Fairall, C., J. Hare, J. Edson, and W. McGillis (2000), Parameterization and micrometeorological measurement of air-sea gas transfer, *Boundary Layer Meteorol.*, *96*(1–2), 63–106, doi:10.1023/A:1002662826020.

Fairall, C. W., E. F. Bradley, D. P. Rogers, J. B. Edson, and G. S. Young (1996), Bulk parameterization of air-sea fluxes for Tropical Ocean-Global Atmosphere Coupled-Ocean Atmosphere Response Experiment, *J. Geophys. Res.*, *101*, 3747–3764.

Gålfalk, M., D. Bastviken, S. Fredriksson, and L. Arneborg (2013), Determination of the piston velocity for water-air interfaces using flux chambers, acoustic Doppler velocimetry, and IR imaging of the water surface, *J. Geophys. Res. Biogeosci.*, *118*, 770–782, doi:10.1002/jgrg.20064.

Gargett, A. E. (1989), Ocean turbulence, *Annu. Rev. Fluid Mech.*, *21*(1), 419–451.

Gemmrich, J. (2012), Bubble-induced turbulence suppression in Langmuir circulation, *Geophys. Res. Lett.*, *39*, L10604, doi:10.1029/2012GL051691.

Goddijn-Murphy, L., D. K. Woolf, and C. Marandino (2012), Space-based retrievals of air-sea gas transfer velocities using altimeters: Calibration for dimethyl sulfide, *J. Geophys. Res.*, *117*, C08028, doi:10.1029/2011JC007535.

Higbie, R. (1935), The rate of absorption of a pure gas into a still liquid during short periods of exposure, *AIChE J.*, *31*, 365–389.

Jähne, B. (2009), Air-sea gas exchange, in *Encyclopedia Ocean Sciences*, edited by J. H. Steele, K. K. Turekian, and S. A. Thorpe, pp. 3434–3444, Elsevier, San Diego, Calif.

Jähne, B., and H. Haußecker (1998), Air-water gas exchange, *Annu. Rev. Fluid Mech.*, *30*(1), 443–468.

Jähne, B., T. Wais, L. Memery, G. Gaulliez, L. Merlivat, K. O. Münnich, and M. Coantic (1985), He and Rn gas exchange experiment in the large wind-wave facility of IMST, *J. Geophys. Res.*, *90*, 11,989–11,998.

Jähne, B., G. Henz, and W. Dietrich (1987), Measurement of the diffusion coefficients of sparingly soluble gases in water, *J. Geophys. Res.*, *92*, 10,767–10,776.

Kitaigorodskii, S. A., M. A. Donelan, J. L. Lumley, and E. A. Terray (1983), Wave-turbulence interactions in the upper ocean: Part II: Statistical characteristics of wave and turbulent components of the random velocity field in the marine surface layer, *J. Phys. Oceanogr.*, *13*, 1988–1999.

Krall, K. E. (2013), Laboratory investigations of air-sea gas transfer under a wide range of water surface conditions, PhD, Ruperto-Carola Univ. of Heidelberg, Germany.

Lamont, J. C., and D. S. Scott (1970), An eddy cell model of mass transfer into the surface of a turbulent liquid, *AIChE J.*, *16*(4), 513–519.

Lana, A., et al. (2011), An updated climatology of surface dimethylsulfide concentrations and emission fluxes in the global ocean, *Global Biogeochem. Cycles*, *25*, GB1004, doi:10.1029/2010GB003850.

Landwehr, S., S. D. Miller, M. J. Smith, E. S. Saltzman, and B. Ward (2013), Analysis of the PKT correction for direct CO_2 flux measurements over the ocean, *Atmos. Chem. Phys.*, *14*, 3361–3372, doi:10.5194/acp-14-3361-2014.

Landwehr, S., N. O'Sullivan, and B. Ward (2015), Direct flux measurements from mobile platforms at sea: Motion and airflow distortion corrections revisited, *J. Atmos. Oceanic Technol.*, *32*, 1163–1178, doi:10.1175/JTECH-D-14-00137.1.

Liss, P. S., and L. Merlivat (1986), The role of air-sea exchange in geochemical cycling, in *Air-Sea Gas Exchange Rates: Introduction and Synthesis*, edited by P. Buat-Menard, pp. 113–127, Kluwer Acad., Dordrecht, Holland.

Lorke, A., and F. Peeters (2006), Toward a unified scaling relation for interfacial fluxes, *J. Phys. Oceanogr.*, *36*(5), 955–961, doi:10.1175/JPO2903.1.

McGillis, W. R., J. B. Edson, J. E. Hare, and C. W. Fairall (2001), Direct covariance air-sea CO_2 fluxes, *J. Geophys. Res.*, *106*, 16,729–16,745.

McGillis, W. R., et al. (2004), Air-sea CO_2 exchange in the equatorial Pacific, *J. Geophys. Res.*, *109*, C08S02, doi:10.1029/2003JC002256.

Miller, S. D., C. Marandino, and E. S. Saltzman (2010), Ship-based measurement of air-sea CO_2 exchange by eddy covariance, *J. Geophys. Res.*, *115*, D02304, doi:10.1029/2009JD012193.

Moog, D. B., and G. H. Jirka (1999), Air-water gas transfer in uniform channel flow, *J. Hydraul. Eng.*, *125*(1), 3–10.

Nightingale, P. D., G. Malin, C. S. Law, A. J. Watson, P. S. Liss, M. I. Liddicoat, J. Boutin, and R. C. Upstill-Goddard (2000), In situ evaluation of air-sea gas exchange parameterizations using novel conservative and volatile tracers, *Global Biogeochem. Cycles*, *14*, 373–387, doi:10.1029/1999GB900091.

O'Sullivan, N., S. Landwehr, and B. Ward (2015), Air-flow distortion and wave interactions on research vessels: An experimental and numerical comparison, *Methods Oceanogr.*, *12*, 1–17, doi:10.1016/j.mio.2015.03.001.

Reichardt, H. (1951), Vollständige Darstellung der turbulenten Geschwindigkeitsverteilung in glatten Leitungen, *ZAMM J. Appl. Math. Mech.*, *7*, 208–219, doi:10.1002/zamm.19510310704.

Richter, K., and B. Jähne (2011), A laboratory study of the Schmidt number dependency of air-water gas transfer, in *Gas Transfer at Water Surfaces 2010*, edited by S. Komori, W. McGillis, and R. Kurose, pp. 322–332, Kyoto Univ. Press, Kyoto.

Saltzman, E. S., W. J. De Bruyn, M. J. Lawler, C. A. Marandino, and C. A. McCormick (2009), A chemical ionization mass spectrometer for continuous underway shipboard analysis of dimethylsulfide in near-surface seawater, *Ocean Sci.*, *5*, 537–546, doi:10.5194/os-5-537-2009.

Scanlon, B., and B. Ward (2013), Oceanic wave breaking coverage separation techniques for active and maturing whitecaps, *Methods Oceanogr.*, *8*, 1–12, doi:10.1016/j.mio.2014.03.001.

Scanlon, B., and B. Ward (2016), The influence of environmental parameters on active and maturing oceanic whitecaps, *J. Geophys. Res. Oceans*, *121*, 3325–3336, doi:10.1002/2015JC011230.

Scanlon, B., O. Breivik, J. R. Bidlot, P. A. E. M. Janssen, A. H. Callaghan, and B. Ward (2016), Modeling whitecap fraction with a wave model, *J. Phys. Oceanogr.*, *46*, 887–894, doi:10.1175/JPO-D-15-0158.1.

Soloviev, A. V., and P. Schlüssel (1994), Parameterization of the cool skin of the ocean and of the air-ocean gas transfer on the basis of modeling surface renewal, *J. Phys. Oceanogr.*, *24*, 1339–1346, doi:10.1175/1520-0485(1994)02 <1339:POTCSO>2.0.CO;2.

Sutherland, G., B. Ward, and K. H. Chrisensen (2013), Wave-turbulence scaling in the ocean mixed layer, *Ocean Sci.*, *9*(4), 597–608, doi:10.5194/os-9-597-2013.

Sutherland, G., K. H. Christensen, and B. Ward (2014a), Evaluating Langmuir turbulence in the oceanic boundary layer, *J. Geophys. Res.*, *119*, 1899–1910, doi:10.1002/2013JC009537.

Sutherland, G., G. Reverdin, L. Marié, and B. Ward (2014b), Mixed and mixing layer depths in the ocean surface boundary layer under conditions of diurnal stratification, *Geophys. Res. Lett.*, *41*, 8469–8476, doi:10.1002/2014GL061939.

Sutherland, P., and W. K. Melville (2015), Field measurements of surface and near-surface turbulence in the presence of breaking waves, *J. Phys. Oceanogr.*, *45*, 943–965, doi:10.1175/JPO-D-14-0133.1.

Sweeney, C., E. Gloor, A. Jacobson, R. Key, G. McKinley, J. Sarmiento, and R. Wanninkhof (2007), Constraining global air-sea gas exchange for CO_2 with recent bomb ^{14}C measurements, *Global Biogeochem. Cycles*, *21*, GB2015, doi:10.1029/2006GB002784.

Terray, E. A., M. A. Donelan, Y. C. Agrawal, W. M. Drennan, K. K. Kahma, A. J. Williams III, P. A. Hwang, and S. A. Kitaigorodskii (1996), Estimates of kinetic energy dissipation under breaking waves, *J. Phys. Oceanogr.*, *26*, 792–807.

Tokoro, T., H. Kayanne, A. Watanabe, K. Nadaoka, H. Tamura, K. Nozaki, K. Kato, and A. Negishi (2008), High gas-transfer velocity in coastal regions with high energy-dissipation rates, *J. Geophys. Res.*, *113*, C11006, doi:10.1029/2007JC004528.

Vachon, D., Y. T. Prairie, and J. J. Cole (2010), The relationship between near-surface turbulence and gas transfer velocity in freshwater systems and its implications for floating chamber measurements of gas exchange, *Limnol. Oceanogr. Methods*, *55*(4), 1723–1732, doi:10.4319/lo.2010.55.4.1723.

Wang, B. Q., and Q. Liao (2016), Field observations of turbulent dissipation rate profiles immediately below the air-water interface, *J. Geophys. Res. Oceans*, *121*, 4377–4391, doi:10.1002/2015JC011512.

Wang, B. Q., Q. Liao, J. H. Fillingham, and H. A. Bootsma (2015), On the coefficients of small eddy and surface divergence models for the air-water gas transfer velocity, *J. Geophys. Res. Oceans*, *120*, 2129–2146, doi:10.1002/2014JC010253.

Wanninkhof, R. (1992), Relationship between wind speed and gas exchange over the ocean, *J. Geophys. Res.*, *97*, 7373–7382.

Wanninkhof, R., and W. R. McGillis (1999), A cubic relationship between air-sea CO_2 exchange and wind speed, *Geophys. Res. Lett.*, *26*(13), 1889–1892, doi:10.1029/19999GL900363.

Wanninkhof, R., W. E. Asher, D. T. Ho, C. Sweeney, and W. R. McGillis (2009), Advances in quantifying air-sea gas exchange and environmental forcing, *Ann. Rev. Mar. Sci.*, *1*, 213–244, doi:10.1146/annurev.marine.010908.163742.

Ward, B. (2007), Air-water interfacial temperature measurements, in *Transport at the Air Sea Interface—Measurements, Models and Parameterizations*, edited by C. S. Garbe, R. A. Handler, and B. Jähne, Springer, Berlin Heidelberg, Germany, doi:10.1007/978-3-540-36906-6_14.

Ward, B., and M. A. Donelan (2006), Thermometric measurements of the molecular sublayer at the air-water interface, *Geophys. Res. Lett.*, *33*, L07605, doi:10.1029/2005GL024769.

Ward, B., T. Fristedt, A. H. Callaghan, G. Sutherland, X. Sanchez, J. Vialand, and A. tenDoeschate (2014), The air-sea interaction profiler for microstructure measurements in the upper ocean, *J. Atmos. Oceanic Technol.*, *31*, 2246–2267, doi:10.1175/JTECH-D-14-00010.1.

Watson, A. J., et al. (2009), Tracking the variable north Atlantic sink for atmospheric CO_2, *Science*, *326*, 1391–1393, doi:10.1126/science.1177394.

Weiss, R. F. (1974), Carbon dioxide in water and seawater: The solubility of a nonideal gas, *Mar. Chem.*, *2*(3), 203–215.

Wu, J. (1971), An estimation of oceanic thermal-sublayer thickness, *J. Phys. Oceanogr.*, *1*, 284–286.

Zappa, C. J., W. R. McGillis, P. A. Raymond, J. B. Edson, E. J. Hintsa, H. J. Zemmelink, J. W. H. Dacey, and D. T. Ho (2007), Environmental turbulent mixing controls on air-water gas exchange in marine and aquatic systems, *Geophys. Res. Lett.*, *34*, L10601, doi:10.1029/2006GL028790.